Masala, Alessio; Vitillo, Jenny; Mondino, Giorgia; Grande, Carlos A.; Blom, Richard; Manzoli, Maela; Marshall, Marc; Bordiga, Silvia. CO2 Capture in Dry and Wet Conditions in UTSA-16 Metal–Organic Framework. ACS APPLIED MATERIALS & INTERFACES. 9 pp: 455-463.
DOI: 10.1021/acsami.6b13216

CO_2 Capture in Dry and Wet Conditions in UTSA-16 Metal-Organic Framework

Alessio Masala[†a], Jenny G. Vitillo[†a], Giorgia Mondino[b], Carlos A. Grande[*b], Richard Blom[b], Maela Manzoli[c], Marc Marshall[d], and Silvia Bordiga[*a]

[a]*Department of Chemistry, NIS and INSTM reference Centres, University of Torino, Via G. Quarello 15/A, 10135 and Via P. Giuria 7, 10125 Torino, Italy.*

[b]*SINTEF Materials and Chemistry, P.O. Box 124 Blindern, N0314 Oslo, Norway.*

[c]*Department of Drug Science and Technology, NIS and INSTM reference Centres, University of Torino, Via Giuria 9, 10125 Torino, Italy*

[d]*School of Chemistry, Monash University, 3800 Victoria, Australia.*

† These authors contributed equally to this paper.

Keywords: UTSA-16; metal-organic frameworks; dry carbon-dioxide capture; wet carbon-dioxide capture MOF-74; post combustion; temperature swing adsorption.

Abstract

Water is the strongest competitor to CO_2 in the adsorption on microporous materials, affecting their performances as CO_2 scrubbers in processes such as post-combustion carbon capture. The metal-organic framework (MOF) UTSA-16 is considered a promising material for its capacity to efficiently capture CO_2 in large quantities, thanks to the presence of open metal sites (OMSs). It is here shown that UTSA-16 is also able to fully desorb water already at room temperature. This property is unique from all the other materials with OMSs reported so far. UTSA-16 retains indeed the 70% of its CO_2 separation capacity after admittance of water in a test flow, created to simulate the emissions from a real post-combustion carbon-capture process. This important aspect not yet observed for any other amine-free material, associated to a high material stability – tested for 160 cycles – and a small temperature swing necessary for regeneration, places UTSA-16 in the restrict number of systems with a real technological future for CO_2 separation.

Introduction

In recent years, Carbon Capture Utilization and Sequestration (CCUS) has emerged as an efficient solution[1] to reduce anthropogenic CO_2 emissions in the atmosphere.[1-5] A novel class of microporous materials with high CO_2 capacity – metal-organic frameworks (MOFs) [6-10] represents a promising alternative to inefficient aqueous alkanolamines, nowadays considered the state of art for CO_2 scrubbers in CCUS processes.[4, 11-14] When designed for post-combustion CO_2 capture, CCUS technology can be easily retrofitted to critical industrial installations such as coal-fueled power plants,[11] which are responsible for 28% of global CO_2 anthropogenic emissions.[15] In the flue gases of this type of plant, CO_2 is mixed in an excess of N_2 (coal-fueled plant exhaust: N_2 73-77%; CO_2 15-16%; H_2O 5-7%;[6, 11] O_2 3-4%; natural gas-fueled plant exhaust: N_2 63-72%; CO_2 8-10%; H_2O 18-20%; O_2 2-3%).[16-17] Besides an efficient screening towards N_2, CO_2 adsorbents – such as microporous materials – must work in the presence of water in order to conceive CCUS for industrial applications. Water represents an important fraction of coal and natural gas-fueled plants flue gas mixture, resulting in a strong competitor to CO_2 due to its high interaction with any material characterized by polarizing centres. As water removal before a CO_2 separation unit would make very unlikely an industrial application of the process,[18] its presence must be seriously taken into account. In MOFs – in addition to the problems related to competitive adsorption on the most reactive sites –[1, 19-20] the presence of water might cause the hydrolysis of the ligand-metal bonds, causing irreversible damage to the crystal structure.[1, 21] This would limit the implementation of MOFs in real CCUS applications. Furthermore, the regeneration (temperature swing) of an adsorber that worked in the presence of moisture,

generally requires temperatures higher than 373 K,[11, 21-24] implying an additional energy demand with respect to an adsorber that worked in dry flow. UTSA-16[25-26] is a MOF with K^+ counter ions as active sites ($K_2Co_3(cit)_2$, see Figure 1a).[27-28] This material shows both high volumetric (160 cm^3 cm^{-3}) and gravimetric CO_2 capacities (4.2 mol kg^{-1} at 1 bar and 298 K; 0.9 mol kg^{-1} at 0.15 bar and 333 K) at 1 bar and 298 K, due to the high concentration of potassium cations and its high density,[26-27] coupled with a low specific heat capacity (1.0-1.4 J $K^{-1}g^{-1}$ between 333 and 423 K)[27] and a medium isosteric heat of CO_2 adsorption.[28] UTSA-16 demonstrated the ability to reversibly adsorb water already at room temperature,[27] like no other MOF with open metal sites (OMSs).

Within this study, a series of single-component (CO_2, H_2O, N_2) sorption isotherms were collected in order to evaluate the technological relevance of UTSA-16 for CCUS in terms of volumetric CO_2 capacity at meaningful pressures, as well as the working capacity and the isosteric heat of adsorption for CO_2, N_2 and H_2O. An evaluation of CO_2/N_2 IAST selectivity has been also addressed. After UTSA-16 saturation with water at 313 K, the material was regenerated with and without temperature swing and the CO_2 capacities were compared. The affinity of UTSA-16 for CO_2 and N_2 was also evaluated by pulse and breakthrough measurements along with their reciprocal diffusion rate constants. The performances of UTSA-16 were then tested by a dynamic experiments aimed to assess the CO_2 separation power of UTSA-16 in a wet gas mixture simulating a post-combustion flue gas (9.83% CO_2, 88.46% N_2, 1.71% H_2O). The results were compared with a dry CO_2/N_2 flow (10% CO_2, 90% N_2) to quantify the effect of the co-presence of water. The dynamic measurements were repeated over 160 adsorption/desorption cycles to test UTSA-16 stability upon prolonged use.

Experimental

Preparation of the sample

UTSA-16 was synthesized as described in the literature.[25-26, 29] Further details are shown in Section S1 of the Supporting Information. If not otherwise specified, UTSA-16 was activated under high vacuum for two hours at room temperature and then heated up to 363 K overnight. Final vacuum was below 5 x 10^{-4} mbar. For the experiments presented in this work, UTSA-16 pellets were prepared by softly pressing the powder at 1 ton and then sieved into macro-particles of 0.2–0.5 mm. The integrity of the UTSA-16 structure was tested by means of XRD, HR-TEM and surface area measurements, as reported in Section S6 of the Supporting Information.

Volumetric CO_2 and N_2 adsorption measurements and isosteric heat of adsorption

CO_2 and N_2 adsorption isotherms were measured using a volumetric instrument (Micromeritics ASAP 2020) on pellet UTSA-16 at 298, 333 and 363 K. An ethylene glycol bath (Julabo EH-25) maintained the isothermal conditions. The CO_2 and N_2 isosteric heats of adsorption were obtained from these isotherms by following the procedure described in Section S2.1 of the Supporting Information. The N_2 isosteric heat of adsorption in Mg_2(dobdc) (Figure S4 of the Supporting Information) was obtained by applying the procedure to the isotherms of Figure S2 of the Supporting Information. Further details are given in Section S2.1 of the Supporting Information.
CO_2/N_2 selectivity factors were evaluated from the CO_2 and N_2 single component isotherms by the Ideal Adsorbed Solution Theory (IAST) using the pyIAST software (Section S2.2 of the Supporting Information)[30-31] or – in a more approximate way – by considering coincident the adsorbed quantities for each gas in the mixture with those of the corresponding pure gas.[11] Eqn. (1) defines the selectivity for two competitor gases:

$$S = \frac{q_i/q_j}{p_i/p_j} \qquad (1)$$

where $q_{i,j}$ represents the quantity of gas i,j adsorbed in mol kg^{-1} and $p_{i,j}$ the partial pressure of the gas i,j.

TSA working capacities were calculated from the 313 K adsorption isotherm (Figure S5a of the Supporting Information) and from the desorption isotherm at 393 K of Figure S5b. The values are reported in Table S6 of the Supporting Information. PSA working capacities were calculated for UTSA-16 isotherms at 313 K (Figure S5a of the Supporting Information) and at 333 K (Figure S5b, blue line). For what concerns the PSA working capacity of Mg_2(dobdc) at 313 K and 333 K, we used the isotherm published by Mason et al.[9] and the one of Figure S2b (black line), respectively. We listed the values in Table S7 of the Supporting Information. More details are listed in Section S2.3 of the Supporting Information.

Gas diffusion study from pulse and breakthrough measurements

Diffusion measurements were performed on pellet UTSA-16 for CO_2 and N_2 at 298, 333, 363 and 393 K. While pulse chromatography was used to measure diffusion of N_2, diffusion parameters of CO_2 were determined by diluted breakthrough experiments. The experimental conditions of both

experiments are listed in Table S8 of the Supporting Information. The flow-rate for diluted CO_2 breakthrough curves (0.5 % CO_2 in He) was fixed at 20 ml/min both for the feed gas and for the helium used for desorption. UTSA-16 was pretreated at 393 K under a flow of helium overnight. Mathematical model used to simulate pulses and breakthrough curves is presented in Section S3.1 of the Supporting Information while further experimental details are listed in Section S3.2 of the Supporting Information. The calculations for the dimensionless Henry's law constants of CO_2 and N_2 are listed in Section S3.2.1 of the Supporting Information

H_2O gravimetric adsorption and isosteric heat of water adsorption

H_2O gravimetric adsorption isotherms were measured on UTSA-16 by means of a Hiden Analytical IGA model IGA-002, at different temperatures (328 and 342 K) to a pressure of 40 mbar. The Henry constants (K_H) [mol kg^{-1} Pa^{-1}] relative to water adsorption were evaluated from the virial fittings of isotherms (see Table S12 in Section S4 of the Supporting Information). The fitted curves of Figure S10 of the Supporting Information were used to evaluate the water isosteric heats of adsorption by following the same procedure described in Section S2.1 of the Supporting Information for CO_2 and N_2 through a fitting of the isotherms with a virial–type equation (see Section S4 of the Supporting Information).

Thermogravimetric analysis at room temperature

The kinetics of water desorption from UTSA-16, reported in Figure 2c were obtained at RT by means of a TA-instruments SDT Q600, under N_2 flux (100 ml min^{-1}) leaving 0.010 g of UTSA-16 placed in an uncovered alumina pan in isothermal conditions for 3 days.

Competitive adsorption of water vapour with CO_2

The sequence of alternate CO_2 (100 mbar) and H_2O (40 mbar) gravimetric single-point adsorption isotherms reported in Figure 2d was measured for 0.02 g of UTSA-16. An intelligent gravimetric analyzer (IGA-002, supplied by Hiden Analytical Ltd, UK) was used, equipped with a fast heating furnace for the temperature control in the 333-673 K range and an ultrahigh vacuum system (10^{-6} mbar). For isothermal measurements at 313 K an isothermal water bath was used. Before each measurement, the sample was degassed for 15 h at 363 K. IGA-002 gravimetric analyser was also used to measure the CO_2 gravimetric isotherms on a wider CO_2 pressure range (0-5 bar) and temperatures (298-393 K, see Figure 4). Before each CO_2 isotherm, a water isotherm was collected at the same temperature. The sample was then reactivated at 363 K before that the following CO_2

isotherm was collected. A detailed description of the experiment is given in Section S5 of the Supporting Information. Figure S12 of the Supporting Information reports the water isotherms at 298, 333, 363 and 393 K measured for this experiment. The CO_2 isotherms were fitted with a cubic spline functions: the fitting curves are reported as continuous lines in Figure 4.

Multicycle stability test in dry and wet conditions

The stability upon cycling was tested by packing 0.471 g of pellet UTSA-16 in a column (5.074 cm length, 0.457 cm diameter) placed in a GC oven connected to an on-line Thermo-mass spectrometer. The aim of this analysis was to evaluate the performances of UTSA-16 as CO_2 adsorbent in presence of a wet gas mixture (9.83% CO_2, 88.46% N_2, 1.71% H_2O) simulating a post-combustion emission exhaust screened by means of temperature swing adsorption (TSA).[32] The procedure followed: i) pure N_2 was injected in the column at 313 K; ii) UTSA-16 was heated up to 393 K in 16 min and kept there for 15 min; iii) the material was then cooled down to 313 K in 16 min; iv) the feed gas was switched to the gas mixture which was put in contact with UTSA-16 for 7 minutes. Steps (i) to (iii) constitute the desorption process while step (iv) describes the adsorption process. This procedure was repeated 160 times (Scheme S1 in Section S6 of the Supporting Information). At the end of the cycling test, the exhaust material was extracted from the column and characterized by using a multi-technique approach as described in Section S6.1, S6.2, S6.3 and S6.4 of the Supporting Information. The same adsorption/desorption procedure described above was followed to study the uptake of CO_2 in dry conditions (10 % CO_2/90% N_2 feed gas composition in step (iv)). For these experiments a NETZSCH STA 449 F1 thermo-gravimeter (TG) connected to a QSM 403 C mass spectrometer was used (see Section S6 of the Supporting Information).

Results and discussion

CO_2 and N_2 single component isotherms

Post-combustion technology requires an adsorber to selectively capture CO_2 in the co-presence of an excess of N_2 (> 60 vol.%). The CO_2 and N_2 single components isotherms for UTSA-16 evaluated at 298, 333 and 363 K at 1 bar are reported in Figure 1b.

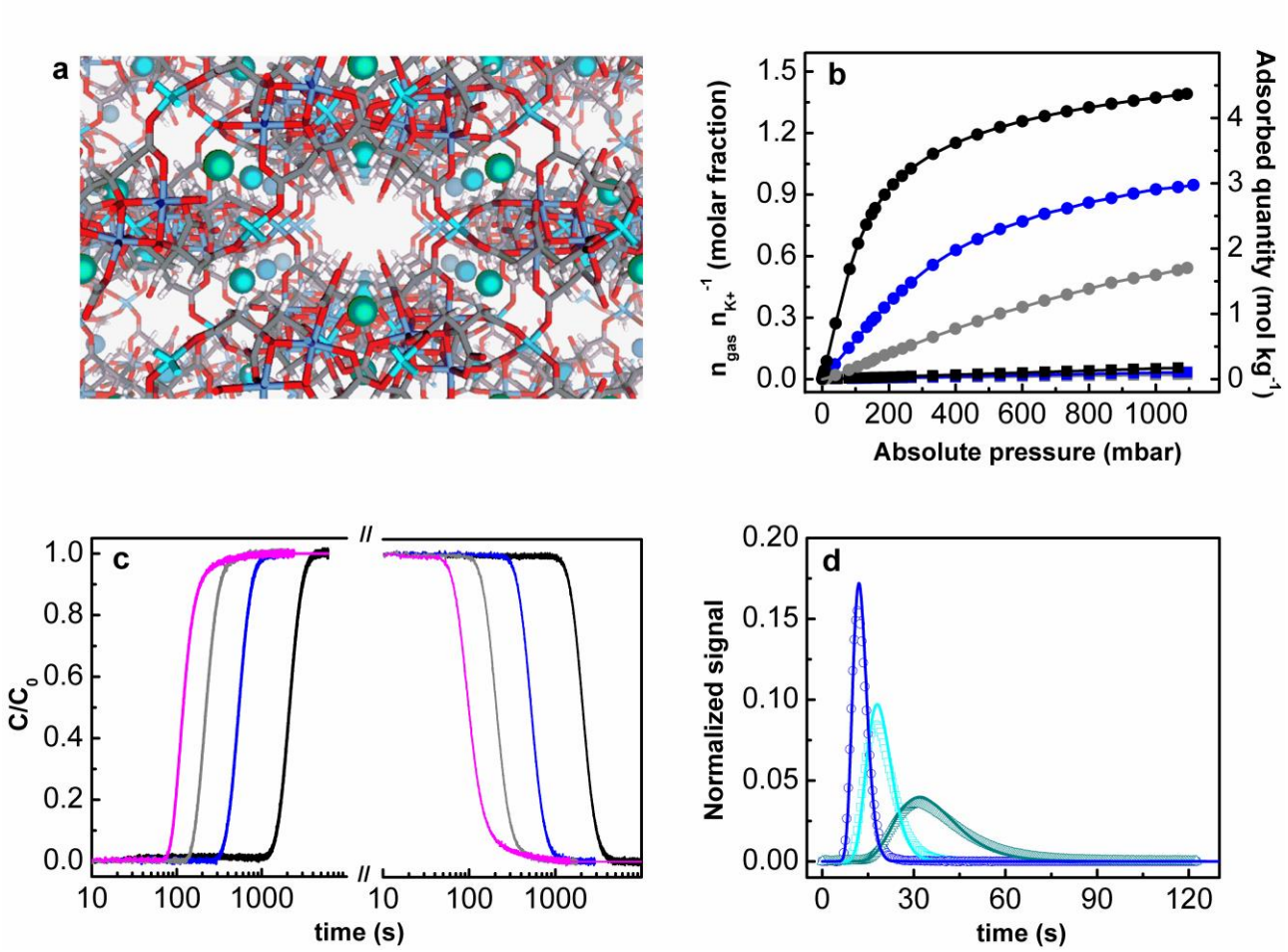

Figure 1 (a) Channel of $[K_2Co_3(cit)_2\ cit=C_6H_4O_7]$ UTSA-16 microporous structure,[25] as view along the [1 0 0] direction. Guest species hosted in the MOF pores were omitted for clarity. The atoms were reported according to the colour code: hydrogen = white, carbon = grey, oxygen = red, tetrahedral cobalt = light blue, octahedral cobalt = violet, potassium = green. (b) CO_2 (●) and N_2 (■) adsorption isotherms at 298 (black line), 333 (blue line) and 363 K (grey line) measured up to 1 bar. Symbols represent experimental data while continuous lines represent the fitted curves, through single or dual-site Langmuir fits (Table S1 and S2 of the Supporting Information). (c) Experimental CO_2 breakthrough adsorption/desorption curves (0.5 % CO_2 in He) on UTSA-16 at 298 (black), 333 (blue), 363 (grey) and 393 K (magenta). X-axis is reported in logarithmic scale. Model data for CO_2 breakthrough experiment are reported in Figure S7 of the Supporting Information. (d) Experimental (symbols) and model (continuous line) data for N_2 pulse chromatography on UTSA-16 at 333 K. The three curves show the signal dependence of the flow: 10 (Δ), 20 (□) and 30 ml min^{-1} (○).

When considering a CO_2/N_2 mixture of 10/90, the uptake of CO_2 on UTSA-16 is one order of magnitude higher than the N_2 capacity for all the temperature considered. The actual loadings at a typical post-combustion temperature (333 K) are 0.6 mol kg^{-1} at 0.10 bar of CO_2 and only 0.09 mol kg^{-1} at 0.90 bar of N_2.[27-28]

The isosteric heat of adsorption (q_{st}) for CO_2 and N_2, are obtained by applying the procedure described in Section S2.1 of the Supporting Information to the isotherm curves of Figure 1b. The heat

involved in the adsorption of CO_2 on UTSA-16 (37 kJ mol^{-1} on average) is consistent with what found in previous works[26-28] and reflects a medium strength physisorption, an important point in order to limit the energy requirements, and hence the cost, of the regeneration process.[11] The interaction energy between CO_2 and UTSA-16 was ca. 24 kJ mol^{-1} higher than those observed for N_2 (Figure S3 and Table S3 of the Supporting Information), so that the average interaction energy for CO_2 (37 kJ mol^{-1}) was more than twice that for N_2 (13 kJ mol^{-1}). Finally, we note that liquefaction heat values for N_2[33] is about 6 kJ mol^{-1}, showing that there was some, albeit weak, interaction between UTSA-16 surface and N_2. It is interesting to note that the isosteric heat of CO_2 adsorption for UTSA-16 approaches the CO_2 q_{st} values found for other important MOFs[34-38] such as Mg_2(dobdc) (Table S3 of the Supporting Information).[39-41]

Apart from its adsorption capacities and enthalpies, an adsorbent must be evaluated towards the diffusion of most relevant gas-mixture components. The reciprocal diffusion time constant (D_c r_c^{-2}),[42] for CO_2 and N_2 were then evaluated by means of diluted breakthrough and pulse chromatography experiments by considering the 298-393 K temperature range, relevant for post-combustion CO_2 capture (see Section S3 of the Supporting Information). Along the reciprocal diffusion time constants (Dc rc^{-2}), the dependence over temperature of the Henry's law constants (K_H) for N_2 and CO_2 was monitored. K_H of each adsorbent–adsorbate pair is strictly linked to the adsorption free energy. Figure 1c shows the diluted breakthrough curves for CO_2 (0.5 % CO_2 in He; see Section S3 of the Supporting Information for experimental details) on UTSA-16 at four different temperatures (298, 333, 363 and 393 K). At the same temperatures used for CO_2, chromatographic experiments were done in order to test the response to pulses of pure N_2 on UTSA-16. In this case, three different flow were considered at each temperature. Figure 1d shows the comparison between simulated and experimental pulses of N_2 at 333 K.

The reciprocal diffusion time constants are reported in Table S11 of the Supporting Information. Interestingly a value of 0.015 s^{-1} was obtained at 333 K for CO_2 indicating a fast diffusion of CO_2 in the UTSA-16 crystals: for comparison, this value is about two orders of magnitude higher than the value of 0.00044 s^{-1} at 323 K reported for the reference material 13X.[42] The D_c r_c^{-2} values obtained for N_2 are two orders of magnitude higher than those obtained for CO_2 because of the lower affinity of UTSA-16 for N_2. Accordingly, the comparison between the dimensionless Henry constants K_H confirms the strong affinity of UTSA-16 towards CO_2 with respect to N_2; as indicated in Figure S9 of the Supporting Information, the K_H relative to CO_2 was more than one order of magnitude higher than for N_2. The N_2 K_H values are almost halved going from 298 to 393 K, whereas they decreases of an order of magnitude for CO_2 in the same temperature range.

From the isotherms of Figure S5a and Figure S5b of the Supporting Information, the working capacity of UTSA-16 were evaluated for TSA and PSA processes. This figure of merit is defined as the amount of CO_2 captured for a complete adsorption/desorption cycle.[9, 32] For a TSA process, the CO_2 working capacity is reported in Table S6. The conditions at which the TSA working capacities were calculated are in line with the one of a post-combustion process, i.e. adsorption at CO_2 partial pressure of 0.15 bar and 313 K and desorption at 1 bar and 393 K.

The TSA working capacity in UTSA-16 were compared to benchmark materials such as Mg_2(dobdc), MOF-177 and NaX zeolite. The data shown in Table S6 illustrates how the UTSA-16 working capacity (0.62 mol kg^{-1}) is similar to the one of NaX zeolite (0.89 mol kg^{-1}) and it is definitely better than MOF-177[9].For what concerns Mg_2(dobdc), this MOF has a working capacity 67% higher than the one of UTSA-16. The supremacy of Mg_2(dobdc) with respect to UTSA-16 in a TSA process, derives from the higher interaction energy towards CO_2 (47 vs. 37 kJ mol^{-1})[39] and to its higher Langmuir surface area (2060 vs. 904 m^2 g^{-1}).[27, 43] However, both Mg_2(dobdc)[24] and NaX[44-46] are highly hydrophilic materials. The UTSA-16 working capacity was evaluated also for a PSA process, as explained in the Section S2.3 of the Supporting Information. A direct comparison was done with Mg_2(dobdc) at 313 and 333 K. In this case, as demonstrated by the values of Table S7 of the Supporting Information, UTSA-16 possesses a PSA working capacity only slightly lower than for Mg_2(dobdc) MOF (-4% at 313 K and -29% at 333 K). The small difference in PSA working capacity between these two MOFs can be related to their different isotherm shapes at the studied temperatures. In fact, while Mg_2(dobdc) has a higher total uptake than UTSA-16 (as shown in Table S7), the latter has a shallower isotherm at the initial step with respect to the former.[11]

H_2O adsorption in UTSA-16

Water adsorption on UTSA-16 was measured at 328 K and it is reported in Figure 2a. This isotherm reassembles the typical trend of microporous materials.[47]

In the experiment, a maximum relative water vapor pressure of 0.25 could be reached (due to instrumental limitations) which corresponds to an absolute pressure of 39 mbar. At this relative water vapor pressure, UTSA-16 was able to uptake 11 mol kg^{-1}, that is slightly lower than what reported for $Cu_3(btc)_2$ in similar conditions (ca. 14 mol kg^{-1}).[34] Looking at the desorption branch (empty symbols in Figure 2a), we note the absence of any hysteresis loop: this indicates on one hand the structure stability of UTSA-16 upon contact with water and, more importantly, the complete removal of water from the material. The ability to efficiently desorb water vapor at a temperature of 328 K was not observed for any other MOFs having OMSs such as Mg_2(dobdc)[24] or $Cu_3(btc)_2$.[24, 34, 48]

The isosteric heat of water on UTSA-16 was extrapolated from the isotherms at 328 and 342 K (Figure S10, Supporting Information) and is plotted as a function of coverage in Figure 2b. In the range of water coverage from 0.08 to 6 mol kg^{-1}, q_{st} increases with increasing coverage, which occurs when the adsorbate-adsorbate (water-water) interaction is greater than the adsorbate-adsorbent interaction.[49-51] When finally a complete monolayer is formed over the adsorbent surface, a maximum in the q_{st} curve is obtained. For UTSA-16, the maximum q_{st} for water molecules was 62 kJ mol^{-1}. This value is lower than what found for water on $Cu_3(btc)_2$ (69.4 kJ mol^{-1})[52] and on a CCUS benchmark MOF such as Mg-MOF-74 (80-73 kJ mol^{-1}),[53-54] explaining the lower activation temperature necessary for UTSA-16.[21] The lower hydrophilicity of UTSA-16 with respect to $Cu_3(btc)_2$ is testified also by the corresponding Henry's law constants (K_H) relative to the interaction of water with the cations: for UTSA-16, K_H was only 8.0 x 10^{-5} mol kg^{-1} Pa^{-1} at 328 K, much lower than K_H for of $Cu_3(btc)_2$ (2.0 x 10^{-2} mol kg^{-1} Pa^{-1} at 323 K).[34, 55]

Complete water removal from UTSA-16 upon degassing was reported also at RT.[27] In Figure 2c, it can be appreciated the kinetics of water removal from UTSA-16 under N_2 flow at RT. This propriety is unique among MOFs possessing OMSs,[24, 34, 48, 56] at which water strongly bound lowering the adsorbent selectivity towards CO_2[57] and vanishing the beneficial effects of these active sites (unless a chemical reaction between the support and CO_2 takes place).[19] This fact would allow to regenerate the material at the same temperature adopted during the adsorption ($\geq$ 313 K), minimizing the temperature swing between adsorption and desorption. For the implementation of these adsorbents in real CCUS applications, the advantages are evident. As a proof of concept, 40 mbar of H_2O was dosed at 313 K on fully activated UTSA-16 in a microbalance. Two activation temperatures were tested: the material was degassed at 363 K and at 313 K until the pristine sample weight was recovered. At 313 K, the sample was fully regenerated upon degassing in less than 2 h (Figure S11, Supporting Information). After equilibration at 313 K, 100 mbar of CO_2 were dosed on UTSA-16.

Figure 2d shows the coincidence between the CO_2 uptakes measured after the activation at 363 K (violet line) and 313 K (light blue line); this indicates how the CO_2 uptake in UTSA-16 does not depend on the treatment temperature. Nevertheless, it is evident from the comparison of Figure 2c and Figure S11 that the time necessary to complete the activation is strongly dependent on temperature. In particular, at room temperature, about 24 h were necessary to remove 88% of the adsorbed water from the material, whereas 2 h were sufficient to complete the process at 313 K. The activation time is further reduced to 30 minutes at 363 K and to less than 10 minutes at 393 K. The regeneration time in UTSA-16 obtained at 393 K is comparable with the one of amine-MOF mmen-Mg_2(dobpdc),[19] which is regenerated in 5 minutes, at 423 K. This result is significant, being alkil-

amine-MOF considered benchmark adsorbents for the capture of CO_2 in the presence of water. These temperatures (363 and 393 K) were chosen to speed up the regeneration step in the cycling measurements reported in the following section.

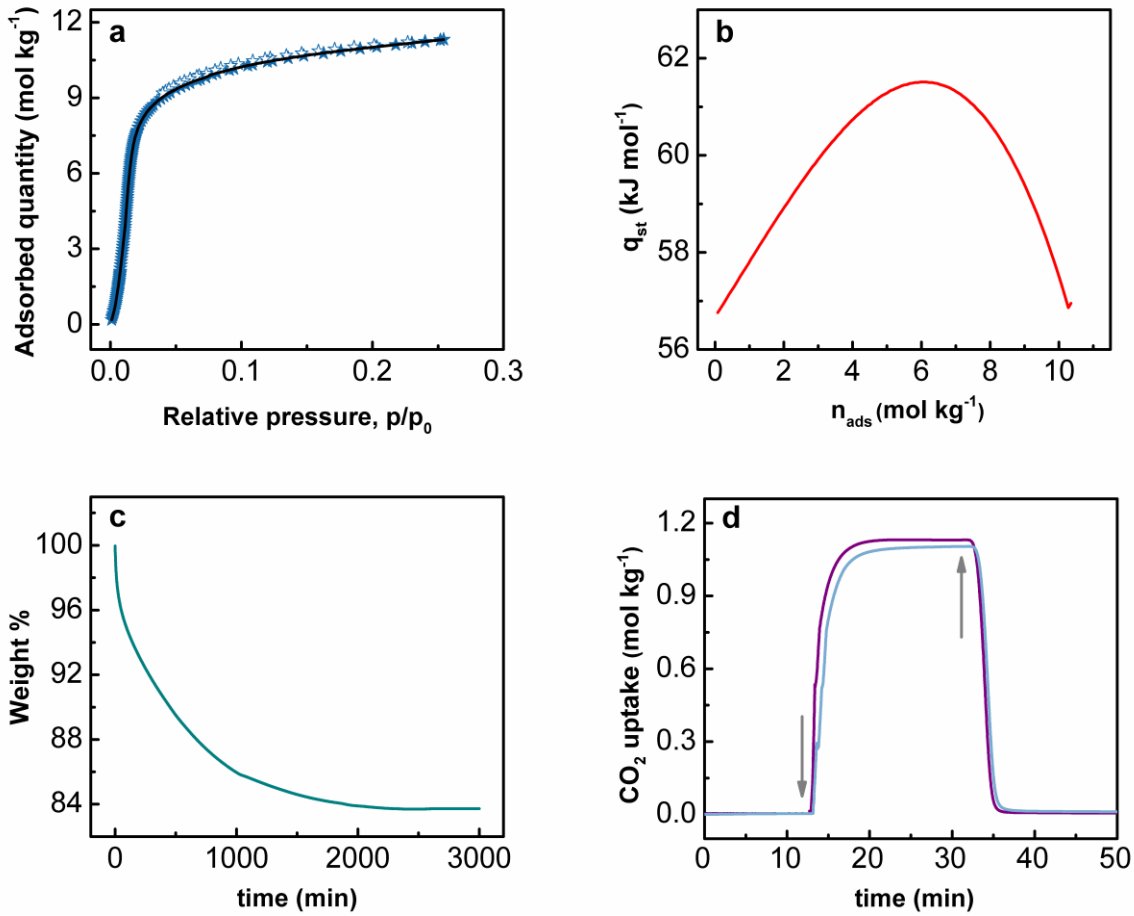

Figure 2 (a) H_2O adsorption isotherm on UTSA-16 at 328 K. Adsorption (★) and desorption (☆) branches are reported. The experimental data were acquired only up to 25% of water saturation, due to instrumental limitations. The black line is the result of the fitting through a virial-type function of the adsorption data (see Section S5 of the Supporting Information). (b) Dependence of the water isosteric heat adsorption to increasing coverage (red line). These points were obtained by applying the procedure of Section S2.1 of the Supporting Information to the water isotherms recorded at 328 and 342 K (Figure S10 of the Supporting Information). (c) Thermogravimetric analysis of UTSA-16 at 298 K under N_2 flow (dark cyan line). (d) Kinetics of CO_2 adsorption cycling on UTSA-16 at 313 K for UTSA-16 activated overnight at 363 K (violet lines) or at 313 K for 2 h after contact with 40 mbar of H_2O (light blue line). A gas pressure of 100 mbar of CO_2 was dosed on the material and, once reached the equilibrium, the system was degassed in dynamic vacuum to verify the reversibility of the process ($p < 1 \times 10^{-3}$ mbar). Up and down arrows mark the starting of the gas dosage and degassing, respectively.

IAST selectivity calculations

The Ideal Adsorbed Solution Theory (IAST) of Myers and Prausnitz[31] has shown to be a reliable method to predict the selectivity of competitor gases that do not strongly interact between each other.[35] In this work, IAST was used to estimate the multi-component isotherms of a CO_2/N_2 mixture, and consequentially the CO_2/N_2 selectivity factors.

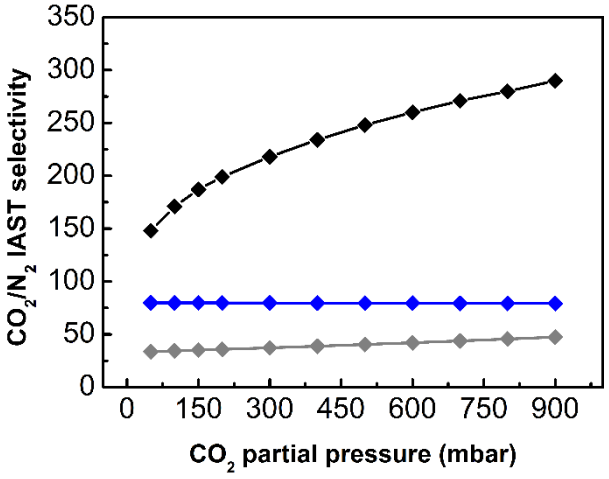

Figure 3 IAST CO_2/N_2 selectivity factors for a CO_2: N_2 binary gas mixture (♦) at 1 bar and 298 (black line), 333 (light blue line) and 363 K (grey line) calculated from experimental single-component isotherms reported in Figure 1b for increasing CO_2 partial pressure.

Figure 3 reports the IAST selectivity factors of CO_2/N_2 gas mixture plotted against increasing CO_2 partial pressure. Focusing the attention on the black curve estimated at 298 K, the UTSA-16 IAST *S* factor relative to 15% CO_2: 85% N_2 is slightly lower than the one obtained at 296 K for the same material, as reported by Xiang et al. (187 vs. 314)[26] where the IAST *S* factors were obtained from simulated single-component isotherms. From the same work of Xiang, it is interesting the matching in *S* factors between Mg_2(dobdc) and UTSA-16 (180 vs. 187). This similarity can be attributed to the CO_2 and N_2 uptakes of UTSA-16 and Mg_2(dobdc) at 0.15 and 0.85 bar, respectively. In fact, at those partial pressures, the higher N_2 uptake in Mg_2(dobdc) with respect to UTSA-16 (1.11 vs. 0.16 mol kg^{-1} at 0.85 bar, Figure 1b and Figure S2a of the Supporting Information), compensate the higher CO_2 uptake in the former with respect to the latter (6.41 vs. 2.53 mol kg^{-1} at 0.85 bar, and Figure 1b and Figure S2b of the Supporting Information).

At 333 K (blue line), the UTSA-16 IAST *S* factor at 15% CO_2 : 85% N_2 decreases as expected, attesting to a value of 80. The use of IAST for the prediction of CO_2 co-adsorption in the presence of water has been avoided in this work. In fact, as demonstrated for adsorbents with similar UTSA-16

properties, a model based on ideal behaviour – such as IAST – cannot properly reproduce the adsorption of CO_2 in the presence of high water vapour concentrations.[58]

Another way to calculate the selectivity is by approximating the adsorbed quantity of each component of the gas mixture by directly extrapolating it from the single components isotherms. Although approximated, this is a method often used in literature as an easy tool for the preliminary screening between different adsorbents. The CO_2/N_2 selectivities of UTSA-16 obtained by this method were reported in Table S5 of the Supporting Information in order to allow the comparison with some of the best adsorbents for CO_2 capture such as $Mg_2(dobdc)$[9] and $Cu_3(btc)_2$[34, 36] (Table S5 and Figure S1 and S2 of the Supporting Information): since the comparison at 333 K is particularly significant for post-combustion processes we point out that, although the maximum CO_2 volumetric capacity of UTSA-16 is lower than that of $Mg_2(dobdc)$ at 1 bar (4.5 vs. 6.1 mmol cm^{-3}, at 333 K), the UTSA-16 CO_2/N_2 is comparable to the one of $Mg_2(dobdc)$[11] and significantly higher than for $Cu_3(btc)_2$.[11]

Stability experiments upon cycling in dry and wet conditions

UTSA-16 stability after repeated contact with water vapour was tested at different adsorption temperatures (T in the 298-393 K range) by measuring the CO_2 isotherm in the over-atmospheric pressure range (0-5 bar). After exposure to water at the T temperature (see Figure S12 of the Supporting Information) the MOF was regenerated at 363 K in vacuum and the CO_2 isotherm was measured. The procedure was repeated at least twice for each temperature (Table S13, Supporting Information). Figure 4 illustrates the full set of gravimetric isotherms of CO_2 collected at increasing temperatures, following the sequence reported in Section S5 of the Supporting Information.

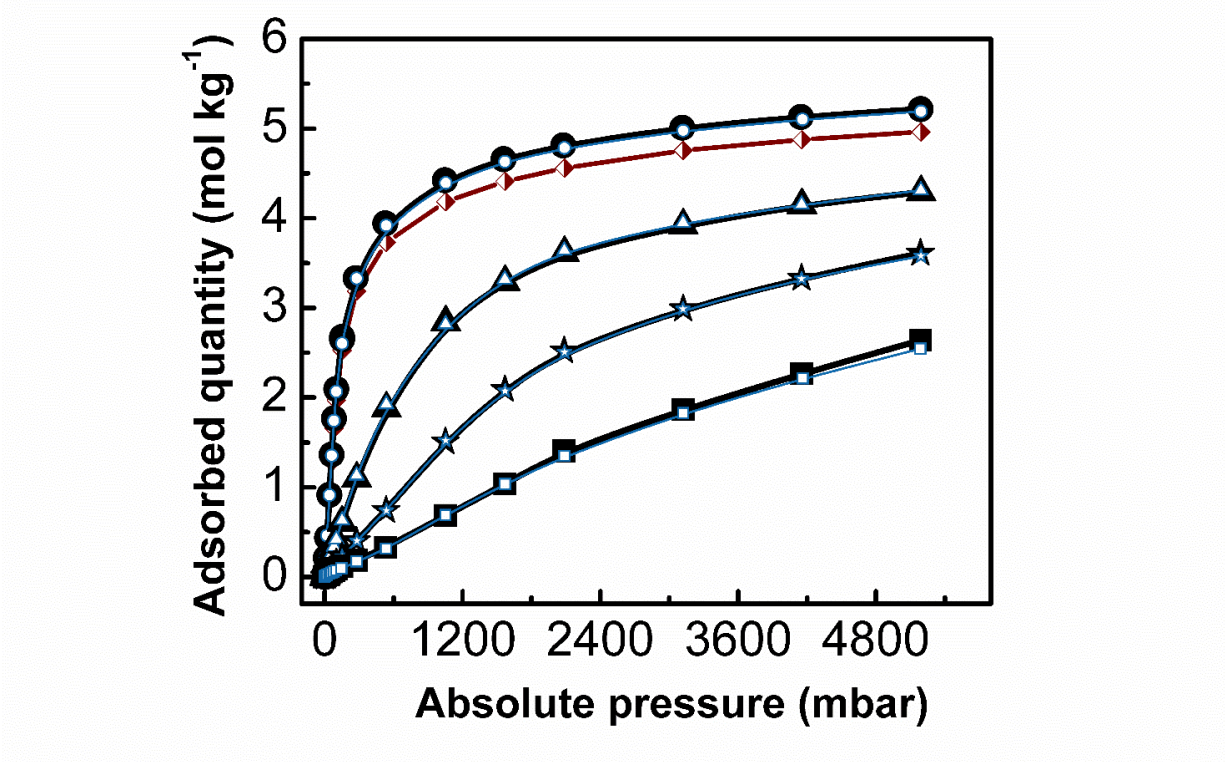

Figure 4 Gravimetric isotherms on UTSA-16 (> 5 bar) at 298 (●), 333 (▲), 363 (★) and 393 K (■) measured for CO_2 before (black line, full symbols) and after (light blue line, empty symbols) contacting the MOF with 40 mbar of water vapour. These isotherms were collected on the same specimen following the sequence: adsCO_2-degas-adsH_2O-degas-adsCO_2. The CO_2 gravimetric isotherm recorded at 298 K after the overall 11 cycles is reported with diamond scatters. Symbols refers to experimental data, continuous lines to the corresponding cubic spline fitting.

The large set of gravimetric isotherms (values listed in Table S13 of the Supporting Information) showed similar behaviour if compared to the volumetric isotherms and illustrates nicely that UTSA-16 is able to uptake the same amount of CO_2 after contact with water vapour at temperatures as high as 393 K (empty symbols, light blue lines). Only the isotherm at 298 K, collected at the end of the entire measurement session, showed a very modest loss (5%) in the CO_2 capture at 5 bar. The uptakes at 0.15 bar (the reference pressure of CO_2 in post combustion emissions) were instead identical from the 1st to the 12th gravimetric isotherm. A very similar experiment reported for $Cu_3(btc)_2$ showed that, already a 298 K and 30% of RH, this MOF undergoes to a continuous loss in CO_2 uptake.[59]

UTSA-16 was tested for vacuum swing adsorption (VSA) by Khurana et al.[60] and Rajagopalan et al.,[61] without considering the effect of water. In our case, cycling experiments (up to 160 cycles) were performed in order to test UTSA-16 stability in a TSA process, in which the presence of water is contemplated. This target was achieved by exposing UTSA-16 to a wet CO_2/N_2 flow at 1 bar and

313 K, simulating the exhaust gas flow coming from a NG-fired power plant: 9.83% CO_2, 88.46% N_2, 1.71% H_2O (see Table S14 and Figure S13 of the Supporting Information). A temperature of 393 K was chosen for a faster desorption of CO_2 in view of the 160 cycles planned for this experiment. By following the composition of the effluent gas over time and comparing the CO_2 breakthrough curves obtained from different cycles it was possible to verify whether the material was able to capture CO_2 in the presence of water vapour and to maintain its structure integrity. A similar experiment was also performed considering a dry 10% CO_2 / 90% N_2 flow, in order to quantify the drop in the CO_2 working capacity due to the presence of water. The results relative to the dry flow are reported in Section S6 of the Supporting Information.

Results obtained for the 1st and the 160th cycle of the wet experiment are shown in Figure 5, and a scheme of the experimental setup (Scheme S1 of the Supporting Information) is reported in Section S6 of the Supporting Information. From Figure 5 it is clear how UTSA-16 maintains its CO_2 capacity in the presence of water vapor, even after 160 cycles. A fortiori, similar results were obtained for the dry flow as shown in Figure S14 of the Supporting Information.

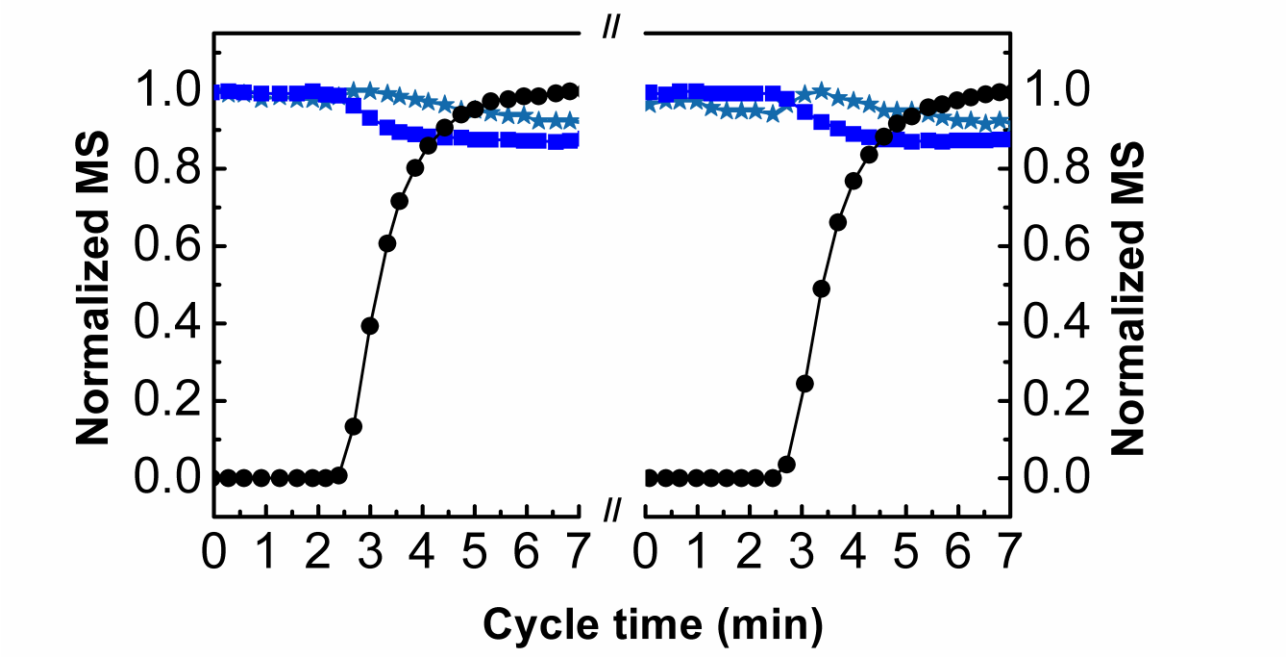

Figure 5 UTSA-16 stability upon cycling as in a TSA process. Mass signals of CO_2 (●, black), N_2 (■) and of water (★, light blue) for the 1st (left) and the 160th cycle (right) of a breakthrough experiment considering a flow of 9.83% CO_2, 88.46% N_2, 1.71% H_2O at 313 K. For a faster moisture removal from the material, the temperature used was 393 K.

A multi-technique approach was used to test the UTSA-16 structural stability after cycling. The structure of UTSA-16 keeps its crystallinity still after cycling as demonstrated by the negligible

changes in XRD patterns (see Figure S15 of the Supporting Information), and the very modest loss in surface area (13%, Table S15 of the Supporting Information) can be compared to the native powder.[27] These results were confirmed by HR-TEM (Figure S16 and S17 of the Supporting Information) that further demonstrated that the cycling processes did not damage the sample.

The CO_2 working capacities for UTSA-16 in wet conditions (0.94 ± 0.04 mol kg^{-1}) are only slightly lower (–31 % in CO_2 uptake) than the working capacity of 1.30 ± 0.02 mol kg^{-1} observed using dry gas feed (Figure S14 of the Supporting Information). Remy et al. performed a similar experiment for Mg_2(dobdc) highlighting a loss in CO_2 capture of 64 % when passing from dry to wet condition.[56] This result is unique among materials in which the capture of CO_2 is not regulated by a chemical reaction. Indeed, for MOFs functionalized with amines (e.g. mmen-Mg_2(dobpdc) and IRMOF-74-III-CH_2NH_2),[19, 62] the uptake of CO_2 does not change after water admittance in the gas flow. Nevertheless, the significantly lower isosteric heat of CO_2 adsorption of UTSA-16 with respect to amine-MOFs (37 vs. 71 kJ mol^{-1}),[63] would lead to a significant reduction in the regeneration costs and in the heat management problems.

Conclusions

Our findings highlighted several important aspects related to UTSA-16 as CO_2 adsorbent. In particular, the presence of water does not affect significantly the CO_2 working capacity of this material when operating in post combustion conditions, even after prolonged cycling, as demonstrated experimentally.

These properties come from the relatively mild affinity of UTSA-16 to water and to the high density of open metal sites, a favorable factor for the interaction with CO_2.

Such a high stability in the CO_2 separation properties was previously reported only for amine-functionalized MOFs. However, this class of MOFs possesses a high CO_2 interaction energy, which leads to a high cost of the adsorbent regeneration and to problems connected with heat management. The lower CO_2 interaction energy of UTSA-16 would allow to overcome the above-mentioned drawbacks typical of amine-functionalized MOFs, making UTSA-16 a competitive material for CO_2 separation not only at academic but also at technological level.

Acknowledgements

The research leading to these results has received funding from the European Union Seventh Framework Programme (FP72007–2013) under Grant Agreement 608534 (MATESA project).

We also acknowledge Prof. Alan Chaffee and Dr. Gregory P. Knowles (School of Chemistry, Monash University, Australia) for useful discussions and help.

Supporting Information

CO_2 isotherm fitting parameters (Table S1); N_2 isotherm fitting parameters (Table S2); sorption properties of $Cu_3(btc)_2$ (Figure S1); sorption properties of $Mg_2(dobdc)$ towards CO_2 and N_2. (Figure S2); CO_2 and N_2 isosteric heat (q_{st}) for different MOFs (Table S3); isosteric heat adsorptions in UTSA-16 (Figure S3); isosteric heat of adsorption. q_{st} of N_2 in $Mg_2(dobdc)$ (Figure S4); IAST selectivity of UTSA-16 towards CO_2/N_2 binary mixture (Table S4); comparison between CO_2/N_2 selectivity factors of different MOFs (Table S5); CO_2 adsorption/desorption isotherms at 313 K and 1 bar on UTSA-16 (Figure S5a); CO_2 adsorption/desorption isotherms at 298, 333, 363 and 393 K and 1 bar on UTSA-16 (Figure S5b); TSA working capacity of UTSA-16, MOF-177, NaX and $Mg_2(dobdc)$ (Table S6); PSA working capacity of UTSA-16 and $Mg_2(dobdc)$ (Table S7); breakthrough experiment parameters (Table S8); CO_2 breakthrough curves at 333 K (Figure S6); CO_2 breakthrough curves (Figure S7); N_2 pulsed chromatographic experiments (Figure S8); CO_2 Henry Constant coefficients (Table S9); N_2 Henry Constant coefficients (Table S10); Comparison between CO_2 and N_2 Henry constants (Figure S9); diffusion measurements outputs (Table S11); H_2O gravimetric adsorption isotherms on UTSA-16 (Figure S10 and Figure S12); H_2O virial-model fitting parameters (Table S12); kinetics of water adsorption on UTSA-16 at 313 K (Figure S11); CO_2 adsorption uptakes for UTSA-16 in the over-atmosphere pressure range (Table S13); stability tests in the presence of moisture (Scheme S1); stability tests in the presence of moisture (Table S14); temperature profile during an adsorption/desorption cycle (Figure S13); stability tests in dry conditions (Figure S14); crystallinity of UTSA-16 after cycling (Figure S15), morphology of UTSA-16 particles (Figure S16); morphology of UTSA-16 particles after cycling (Figure S17); Langmuir surface area and pore's volume of UTSA-16 (Table S15); CO_2 adsorption on UTSA-16 particles after cycling (Figure S18).

Author Information

Corresponding Author:
e-mail: silvia.bordiga@unito.it; telephone:0039 011 6708373

Bibliography

1. Vitillo, J. G., Magnesium-Based Systems for Carbon Dioxide Capture, Storage and Recycling: From Leaves to Synthetic Nanostructured Materials. *RSC Adv.* **2015,** *5* (46), 36192-36239.
2. Edenhofer, O.; Pichs-Madruga, R.; Sokona, Y.; Farahani, E.; Kadner, S.; Seyboth, K.; Adler, A.; Baum, I.; Brunner, S.; Eickemeier, P.; Kriemann, B.; Savolainen, J.; Schlömer, S.; von Stechow, C.; Zwickel, T.; and Minx, J. C., *IPCC Fifth Assessment Report, Intergovernmental Panel on Climate Change*. Cambridge University Press: Cambridge, United Kingdom and New York, NY, USA, **2014**.
3. US-NOAA, Earth System Research Laboratory. http://www.esrl.noaa.gov (accessed August).
4. Rochelle, G. T., Amine Scrubbing for CO_2 Capture. *Science* **2009,** *325* (5948), 1652-1654.
5. UNFCCC, *Adoption of the Paris Agreement COP 21*. Paris, **2015**.
6. Granite, E. J.; Pennline, H. W., Photochemical Removal of Mercury from Flue Gas. *Ind. Eng. Chem. Res.* **2002,** *41* (22), 5470-5476.
7. Jassim, M. S.; Rochelle, G. T., Innovative Absorber/Stripper Configurations for CO_2 Capture by Aqueous Monoethanolamine. *Ind. Eng. Chem. Res.* **2006,** *45* (8), 2465-2472.
8. Lee, K. B.; Sircar, S., Removal and Recovery of Compressed CO_2 from Flue Gas by a Novel Thermal Swing Chemisorption Process. *Aiche Journal* **2008,** *54* (9), 2293-2302.
9. Mason, J. A.; Sumida, K.; Herm, Z. R.; Krishna, R.; Long, J. R., Evaluating Metal-Organic Frameworks for Post-Combustion Carbon Dioxide Capture Via Temperature Swing Adsorption. *Energy Environ. Sci.* **2011,** *4* (8), 3030-3040.
10. Zhang, Z. J.; Yao, Z. Z.; Xiang, S. C.; Chen, B. L., Perspective of Microporous Metal-Organic Frameworks for CO_2 Capture and Separation. *Energy Environ. Sci.* **2014,** *7* (9), 2868-2899.
11. Sumida, K.; Rogow, D. L.; Mason, J. A.; McDonald, T. M.; Bloch, E. D.; Herm, Z. R.; Bae, T. H.; Long, J. R., Carbon Dioxide Capture in Metal-Organic Frameworks. *Chem. Rev.* **2012,** *112* (2), 724-781.
12. Davis, J. D. Thermal Degradation of Aqueous Amines Used for Carbon Dioxide Capture. University of Texas, Austin, **2009**.
13. Haszeldine, R. S., Carbon Capture and Storage: How Green Can Black Be? *Science* **2009,** *325* (5948), 1647-1652.
14. Veawab, A.; Tontiwachwuthikul, P.; Chakma, A., Corrosion Behavior of Carbon Steel in the CO_2 Absorption Process Using Aqueous Amine Solutions. *Ind. Eng. Chem. Res.* **1999,** *38* (10), 3917-3924.
15. *Power Generation from Coal*. International Energy Agency: Paris, **2010**; p 111.
16. Park, S. E.; Chang, J. S.; Lee, K. W., *Carbon Dioxide Utilization for Global Sustainability: Proceedings of the 7th International Conference on Carbon Dioxide Utilization*. Elsevier: Amsterdam, **2004**; p 626.
17. Song, C. S.; Pan, W., Tri-Reforming of Methane: A Novel Concept for Synthesis of Industrially Useful Syngas with Desired H_2/CO Ratios Using Flue Gas of Power Plants without CO_2 Pre-Separation. *Abstr. Pap. Am. Chem. Soc.* **2004,** *227*, 128-131.
18. Keskin, S.; van Heest, T. M.; Sholl, D. S., Can Metal-Organic Framework Materials Play a Useful Role in Large-Scale Carbon Dioxide Separations? *ChemSusChem* **2010,** *3* (8), 879-891.
19. McDonald, T. M.; Mason, J. A.; Kong, X. Q.; Bloch, E. D.; Gygi, D.; Dani, A.; Crocella, V.; Giordanino, F.; Odoh, S. O.; Drisdell, W. S.; Vlaisavljevich, B.; Dzubak, A. L.; Poloni, R.; Schnell, S. K.; Planas, N.; Lee, K.; Pascal, T.; Wan, L. W. F.; Prendergast, D.; Neaton, J.

B.; Smit, B.; Kortright, J. B.; Gagliardi, L.; Bordiga, S.; Reimer, J. A.; Long, J. R., Cooperative Insertion of CO_2 in Diamine-Appended Metal-Organic Frameworks. *Nature* **2015,** *519* (7543), 303-308.
20. Tan, K.; Zuluaga, S.; Gong, Q. H.; Gao, Y. Z.; Nijem, N.; Li, J.; Thonhauser, T.; Chabal, Y. J., Competitive Coadsorption of CO_2 with H_2O, NH_3, SO_2, NO, NO_2, N_2, O_2, and CH_4 in M-MOF-74 (M = Mg, Co, Ni): The Role of Hydrogen Bonding. *Chem. Mat.* **2015,** *27* (6), 2203-2217.
21. Low, J. J.; Benin, A. I.; Jakubczak, P.; Abrahamian, J. F.; Faheem, S. A.; Willis, R. R., Virtual High Throughput Screening Confirmed Experimentally: Porous Coordination Polymer Hydration. *J. Am. Chem. Soc.* **2009,** *131* (43), 15834-15842.
22. Liu, J.; Wang, Y.; Benin, A. I.; Jakubczak, P.; Willis, R. R.; LeVan, M. D., CO_2/H_2O Adsorption Equilibrium and Rates on Metal-Organic Frameworks: HKUST-1 and Ni/Dobdc. *Langmuir* **2010,** *26* (17), 14301-14307.
23. Choi, H. J.; Dinca, M.; Dailly, A.; Long, J. R., Hydrogen Storage in Water-Stable Metal-Organic Frameworks Incorporating 1,3-and 1,4-benzenedipyrazolate. *Energy Environ. Sci.* **2010,** *3* (1), 117-123.
24. Schoenecker, P. M.; Carson, C. G.; Jasuja, H.; Flemming, C. J. J.; Walton, K. S., Effect of Water Adsorption on Retention of Structure and Surface Area of Metal-Organic Frameworks. *Ind. Eng. Chem. Res.* **2012,** *51* (18), 6513-6519.
25. Xiang, S. C.; Wu, X. T.; Zhang, J. J.; Fu, R. B.; Hu, S. M.; Zhang, X. D., A 3D Canted Antiferromagnetic Porous Metal-Organic Framework with Anatase Topology through Assembly of an Analogue of Polyoxometalate. *J. Am. Chem. Soc.* **2005,** *127* (47), 16352-16353.
26. Xiang, S. C.; He, Y. B.; Zhang, Z. J.; Wu, H.; Zhou, W.; Krishna, R.; Chen, B. L., Microporous Metal-Organic Framework with Potential for Carbon Dioxide Capture at Ambient Conditions. *Nat. Commun.* **2012,** *3*, 953-962.
27. Masala, A.; Vitillo, J. G.; Bonino, F.; Manzoli, M.; Grande, C. A.; Bordiga, S., New Insights into UTSA-16. *Phys. Chem. Chem. Phys.* **2016,** *18* (1), 220-227.
28. Masala, A.; Grifasi, F.; Atzori, C.; Vitillo, J. G.; Mino, L.; Bonino, F.; Chierotti, M. R.; Bordiga, S., CO_2 Adsorption Sites in UTSA-16: Multitechnique Approach *J. Phys. Chem. C* **2016,** *120* (22), 12068-12074.
29. Grande, C. A.; Agueda, V. I.; Spjelkavik, A.; Blom, R., An Efficient Recipe for Formulation of Metal-Organic Frameworks. *Chem. Eng. Sci.* **2014,** *124*, 154-158.
30. Simon, C. M.; Smit, B.; Haranczyk, M., Pyiast: Ideal Adsorbed Solution Theory (IAST) Python Package. *Comput. Phys. Commun.* **2016,** *200*, 364-380.
31. Myers, A. L.; Prausnitz, J. M., Thermodynamics of Mixed-Gas Adsorption. *Aiche Journal* **1965,** *11* (1), 121-127.
32. Berger, A. H.; Bhown, A. S., Comparing Physisorption and Chemisorption Solid Sorbents for Use Separating CO_2 from Flue Gas Using Temperature Swing Adsorption. In *10th International Conference on Greenhouse Gas Control Technologies*, Gale, J.; Hendriks, C.; Turkenberg, W., Eds. Elsevier Science Bv: Amsterdam, **2011**, pp 562-567.
33. Haynes, W. M., *Crc Handbook of Chemistry and Physics*. Boca Raton, Florida, **2003**; Vol. 84th.
34. Al-Janabi, N.; Hill, P.; Torrente-Murciano, L.; Garforth, A.; Gorgojo, P.; Siperstein, F.; Fan, X. L., Mapping the Cu-btc Metal-Organic Framework (HKUST-1) Stability Envelope in the Presence of Water Vapour for CO_2 Adsorption from Flue Gases. *Chem. Eng. J.* **2015,** *281*, 669-677.
35. Simmons, J. M.; Wu, H.; Zhou, W.; Yildirim, T., Carbon Capture in Metal-Organic Frameworks-a Comparative Study. *Energy Environ. Sci.* **2011,** *4* (6), 2177-2185.

36. Wang, Q. M.; Shen, D. M.; Bulow, M.; Lau, M. L.; Deng, S. G.; Fitch, F. R.; Lemcoff, N. O.; Semanscin, J., Metallo-Organic Molecular Sieve for Gas Separation and Purification. *Microporous Mesoporous Mat.* **2002,** *55* (2), 217-230.
37. Yang, Q. Y.; Xue, C. Y.; Zhong, C. L.; Chen, J. F., Molecular Simulation of Separation of CO_2 from Flue Gases in Cu-btc Metal-Organic Framework. *Aiche Journal* **2007,** *53* (11), 2832-2840.
38. Dietzel, P. D. C.; Johnsen, R. E.; Fjellvag, H.; Bordiga, S.; Groppo, E.; Chavan, S.; Blom, R., Adsorption Properties and Structure of CO_2 Adsorbed on Open Coordination Sites of Metal-Organic Framework Ni_2(dhtp) from Gas Adsorption, IR Spectroscopy and X-Ray Diffraction. *Chem. Commun.* **2008,** (41), 5125-5127.
39. Caskey, S. R.; Wong-Foy, A. G.; Matzger, A. J., Dramatic Tuning of Carbon Dioxide Uptake Via Metal Substitution in a Coordination Polymer with Cylindrical Pores. *J. Am. Chem. Soc.* **2008,** *130* (33), 10870-10871.
40. Dietzel, P. D. C.; Besikiotis, V.; Blom, R., Application of Metal-Organic Frameworks with Coordinatively Unsaturated Metal Sites in Storage and Separation of Methane and Carbon Dioxide. *J. Mater. Chem.* **2009,** *19* (39), 7362-7370.
41. Britt, D.; Furukawa, H.; Wang, B.; Glover, T. G.; Yaghi, O. M., Highly Efficient Separation of Carbon Dioxide by a Metal-Organic Framework Replete with Open Metal Sites. *Proc. Natl. Acad. Sci. U. S. A.* **2009,** *106* (49), 20637-20640.
42. Delgado, J. A.; Agueda, V. I.; Uguina, M. A.; Sotelo, J. L.; Brea, P.; Grande, C. A., Adsorption and Diffusion of H_2/CO, CH_4, and CO_2 in Bpl Activated Carbon and 13X Zeolite: Evaluation of Performance in Pressure Swing Adsorption Hydrogen Purification by Simulation. *Ind. Eng. Chem. Res.* **2014,** *53* (40), 15414-15426.
43. Herm, Z. R.; Swisher, J. A.; Smit, B.; Krishna, R.; Long, J. R., Metal-Organic Frameworks as Adsorbents for Hydrogen Purification and Precombustion Carbon Dioxide Capture. *J. Am. Chem. Soc.* **2011,** *133* (15), 5664-5667.
44. Li, G.; Xiao, P.; Webley, P.; Zhang, J.; Singh, R.; Marshall, M., Capture of CO_2 from High Humidity Flue Gas by Vacuum Swing Adsorption with Zeolite 13X. *Adsorption-Journal of the International Adsorption Society* **2008,** *14* (2-3), 415-422.
45. Shen, C. M.; Worek, W. M., Cosorption Characteristics of Solid Adsorbents. *Int. J. Heat Mass Transf.* **1994,** *37* (14), 2123-2129.
46. Bezerra, D. P.; Oliveira, R. S.; Vieira, R. S.; Cavalcante, C. L.; Azevedo, D. C. S., Adsorption of CO_2 on Nitrogen-Enriched Activated Carbon and Zeolite 13X. *Adsorption-Journal of the International Adsorption Society* **2011,** *17* (1), 235-246.
47. Lowell, S.; Shields, J. E.; Thomas, M. A.; Thommes, M., *Characterization of Porous Solids and Powders: Surface Area, Pore Size and Density*. Springer Science & Business Media: New York, **2012**; Vol. 12, p 350.
48. Kusgens, P.; Rose, M.; Senkovska, I.; Frode, H.; Henschel, A.; Siegle, S.; Kaskel, S., Characterization of Metal-Organic Frameworks by Water Adsorption. *Microporous Mesoporous Mat.* **2009,** *120* (3), 325-330.
49. Hernandez-Huesca, R.; Diaz, L.; Aguilar-Armenta, G., Adsorption Equilibria and Kinetics of CO_2, CH_4 and N_2 in Natural Zeolites. *Sep. Purif. Technol.* **1999,** *15* (2), 163-173.
50. Aguilar-Armenta, G.; Patino-Iglesias, M. E.; Jimenez-Jimenez, J.; Rodriguez-Castellon, E.; Jimenez-Lopez, A., Application of Porous Phosphate Heterostructure Materials for Gas Separation. *Langmuir* **2006,** *22* (3), 1260-1267.
51. Dominguez, G.; Hernandez-Huesca, R.; Aguilar-Armenta, G., Isosteric Heats of Adsorption of N_2O and NO on Natural Zeolites. *J. Mex. Chem. Soc.* **2010,** *54* (2), 111-116.
52. Bhunia, M. K.; Hughes, J. T.; Fettinger, J. C.; Navrotsky, A., Thermochemistry of Paddle Wheel MOFs: Cu-HKUST-1 and Zn-HKUST-1. *Langmuir* **2013,** *29* (25), 8140-8145.

53. Yu, K.; Kiesling, K.; Schmidt, J. R., Trace Flue Gas Contaminants Poison Coordinatively Unsaturated Metal-Organic Frameworks: Implications for CO_2 Adsorption and Separation. *J. Phys. Chem. C* **2012,** *116* (38), 20480-20488.
54. Canepa, P.; Arter, C. A.; Conwill, E. M.; Johnson, D. H.; Shoemaker, B. A.; Soliman, K. Z.; Thonhauser, T., High-Throughput Screening of Small-Molecule Adsorption in MOF. *J. Mater. Chem. A* **2013,** *1* (43), 13597-13604.
55. Castillo, J. M.; Vlugt, T. J. H.; Calero, S., Understanding Water Adsorption in Cu-btc Metal-Organic Frameworks. *J. Phys. Chem. C* **2008,** *112* (41), 15934-15939.
56. Remy, T.; Peter, S. A.; Van der Perre, S.; Valvekens, P.; De Vos, D. E.; Baron, G. V.; Denayer, J. F. M., Selective Dynamic CO_2 Separations on Mg-MOF-74 at Low Pressures: A Detailed Comparison with 13X. *J. Phys. Chem. C* **2013,** *117* (18), 9301-9310.
57. Woerner, W. R.; Plonka, A. M.; Chen, X. Y.; Banerjee, D.; Thallapally, P. K.; Parise, J. B., Simultaneous in Situ X-Ray Diffraction and Calorimetric Studies as a Tool to Evaluate Gas Adsorption in Microporous Materials. *J. Phys. Chem. C* **2016,** *120* (1), 360-369.
58. Wang, Y.; Levan, M. D., Adsorption Equilibrium of Binary Mixtures of Carbon Dioxide and Water Vapor on Zeolites 5a and 13X. *J. Chem. Eng. Data* **2010,** *55* (9), 3189-3195.
59. Liang, Z. J.; Marshall, M.; Chaffee, A. L., CO_2 Adsorption-Based Separation by Metal Organic Framework (Cu-btc) Versus Zeolite (13X). *Energy Fuels* **2009,** *23*, 2785-2789.
60. Khurana, M.; Farooq, S., Simulation and Optimization of a 6-Step Dual-Reflux VSA Cycle for Post-Combustion CO_2 Capture. *Chem. Eng. Sci.* **2016,** *152*, 507-515.
61. Rajagopalan, A. K.; Avila, A. M.; Rajendran, A., Do Adsorbent Screening Metrics Predict Process Performance? A Process Optimisation Based Study for Post-Combustion Capture of CO_2. *Int. J. Greenh. Gas Control* **2016,** *46*, 76-85.
62. Fracaroli, A. M.; Furukawa, H.; Suzuki, M.; Dodd, M.; Okajima, S.; Gandara, F.; Reimer, J. A.; Yaghi, O. M., Metal-Organic Frameworks with Precisely Designed Interior for Carbon Dioxide Capture in the Presence of Water. *J. Am. Chem. Soc.* **2014,** *136* (25), 8863-8866.
63. McDonald, T. M.; Lee, W. R.; Mason, J. A.; Wiers, B. M.; Hong, C. S.; Long, J. R., Capture of Carbon Dioxide from Air and Flue Gas in the Alkylamine-Appended Metal-Organic Framework Mmen-Mg_2(Dobpdc). *J. Am. Chem. Soc.* **2012,** *134* (16), 7056-7065.

GRAPHICAL ABSTRACT

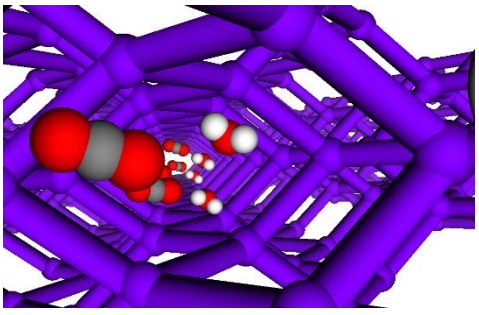

UTSA-16 metal-organic framework showed applicability-level selectivity towards CO_2 in real post-combustion flue gas conditions.